Application of Analytical Centrifugation to Chemical Systems for Measurement of Properties and Phase Equilibria

Kotaro Oshima, Kentaro Nakamura, Natsuki Sato, Haixin Guo and Richard Smith*

Graduate School of Environmental Studies, Tohoku University
Aramaki Aza Aoba 6-6-11-413, Aoba-ku, Sendai 980-8579, Japan

* To whom correspondence should be addressed.
Email: smith@scf.che.tohoku.ac.jp Tel: 022-795-5863 FAX: 022-795-5864

Abstract

In this mini-review, fundamentals and techniques of analytical centrifugation (AC) and analytical ultracentrifugation (AUC) are highlighted and their applications to property determination and to fluid phase equilibria are discussed. AC/AUC techniques allow determination of nanoparticle properties such as particle density, molecular weight, particle size distribution, diffusion coefficients, nanoparticle coating or capping thickness, particle association, species aggregation, geometric factors, and particle frictional coefficients. In the study of fluid phase equilibria, AC/AUC techniques have been used to determine the osmotic pressure equation of state for ferrofluids, colloidal systems (clays, polystyrene, photonic material self-assembly) and the techniques have application to the determination of solid-liquid equilibria of mass transfer limited (high viscosity) chemical systems such as deep eutectic solvents and ionic liquids and process intensification devices such as centrifugal contactor separators. AC/AUC techniques allow the study of the properties and phase equilibria of many types of biological and chemical systems and will greatly broaden the scope of research into fluid phase equilibria.

Keywords: experimental technique, nanotechnology, process intensification, osmotic pressure, colloids, solid-liquid equilibria

1. Introduction

Analytical centrifugation (AC) and analytical ultracentrifugation (AUC) are techniques that optically monitor the translational motion of molecular species in a solution during application of a gravitational field. In this text, AC refers to instruments that can apply gravitational fields of less than 4000*g* while AUC refers to instruments that can apply gravitational fields of 250000*g* or higher. In AC and AUC instrumentation, factors as multiples of Earth gravity, *g*, called the G-force (G) or relative centrifugal force (RCF) are used to describe the centrifugal force ($F=m\omega^2 r$) on a sample according to rotor radius, *r* (m), and rotor speed (rpm) in revolutions per minute:

$$G\text{-force} = \text{RCF} = \frac{\omega^2 r}{g} = 1.1179 \cdot 10^{-3} \cdot r \cdot (\text{rotor speed})^2 \tag{1}$$

The geometry of the instruments can be a rotating cylinder, a rotating assembly that contains sample cells (i.e. typical laboratory centrifuge) or a flat rotating disk. Both AC and AUC techniques allow study of proteins, macromolecules, viruses, DNA, fine particles and nanoparticles in their native solutions or in chemical systems that are of biological or technological interest and they share the same rigorous thermodynamic basis developed by Svedberg and Rinde [1]. AC and AUC have evolved according to advances in instrumentation, theory and software as brought out in a lucid review on globular macromolecules by Winzor et al. [2]. In this mini-review, fundamentals of AC/AUC are highlighted and applications are discussed as applied to chemical systems including fluid phase equilibria.

1.1 Fundamental definitions

When a molecular species in a sample cell, either in solution or as a dispersion, is subjected to centrifugal force, translation of the molecular species occurs according to a balance of sedimenting, bouyancy and frictional forces. The acceleration in the system is given by the distance of the molecular species from the axis of rotation, *r*, multiplied by the square of the angular velocity, ω, whereas the ratio of the velocity of the molecular species, *u*, to the given acceleration, $\omega^2 r$, is called the sedimentation coefficient, *s*, defined as:

$$s \equiv \frac{u}{\omega^2 r} = \frac{m_P(1-(\rho_S/\rho_P))}{f} = \frac{Dm_P(1-(\rho_S/\rho_P))}{k_B T} \tag{2}$$

In eq. (2), *s* is proportional to the effective (buoyant) particle mass, m_P, and inversely proportional to the orientation-averaged frictional coefficient, *f*, of the molecular species, while ρ_P is the particle density, ρ_S is the solvent density, k_B is Boltzmann's constant and *D* is the diffusion coefficient. The sedimentation coefficient defined in eq. (2) has units of time that is typically on the order of 10^{-13} s for proteins or Svedberg (S) units, where 1 S = 10^{-13} s, is used to represent *s* values (e.g. s^0 = 7.38 S for equine γ-globulin [2]) corrected to 20 ºC.

When a centrifugal force is applied to particles in solution, sedimenting, buoyancy and

frictional forces attain steady-state values rapidly (~10^{-6} s) and translation of particles occurs at terminal velocity [3]. For a frictional coefficient given by Stokes' law at infinite dilution, the sedimentation coefficient can be written as [4]:

$$s = \frac{d_h^2(\rho_P - \rho_S)}{18\mu_S} \tag{3}$$

where d_h is the hydrodynamic particle diameter and μ_S is the solvent viscosity. As conditions deviate from concentrations at infinite dilution (c = 0), the frictional coefficient, as well as the diffusion coefficient, becomes a function of mass concentration as a first-order approximation,

$$f = f_0(1 + k_s c) \tag{4}$$

where f_0 is the frictional (Stokes' law) coefficient at infinite dilution, c is the mass based concentration and k_S is the Gralen coefficient, which is related to the concentration. The sedimentation coefficient can be written in terms of the volume fraction as:

$$s = \frac{s_0}{1 + K_s\varphi_P} \quad where \;\; K_s = \frac{k_s}{v_s} \tag{5}$$

where the 0 subscript denotes infinite dilution, φ_P is the volume fraction of the particles and v_S is the swollen particle specific volume that accounts for entrained solvent around the particle as it moves through the solvent phase [4].

In the parameter-free approach, eq. (3) can be rearranged to give an effective hydrodynamic diameter of the molecular species as they move through the chemical system:

$$d_h = \sqrt{\frac{18\mu_S s}{(\rho_P - \rho_S)}} \tag{6}$$

AC instruments that use eq. (6) can provide an immediate hydrodynamic diameter of the chemical species based on the range of sedimentation coefficients measured.

When AC or AUC is applied to sample at appropriate conditions, a sedimentation front develops that separates the chemical system into a sediment region, a boundary region (dispersed phase) and a supernatant region. The optical absorbance (or transmittance) of the sediment region is called the plateau concentration (c_P), whereas the boundary region has a range of compositions that vary logarithmically from c_0 to c_P at a distance that is measured relative to the meniscus of the solvent in the cell (r_m) and the moving front in the boundary region (r_b), which in an integrated form is written as,

$$s^*(t) = \frac{dr/dt}{\omega^2 r} = \frac{\ln(r_b / r_m)}{\omega^2 t} \tag{7}$$

where s^* is a time-dependent apparent sedimentation coefficient (* denotes apparent) that results from the concentration dependence of the moving boundary region and its distribution function is known as $g^*(s)$.

The Lamm equation [5] is a mass conservation equation that describes the sedimentation and diffusion of particles under centrifugal force:

$$\frac{\partial c}{\partial t} = D\left(\frac{\partial^2 c}{\partial r^2} + \frac{1}{r}\cdot\frac{\partial c}{\partial r}\right) - \omega^2 s\left(r\frac{\partial c}{\partial r} + 2c\right) \tag{8}$$

In eq. (8), D is the concentration dependent diffusion coefficient and $\partial c / \partial t$ is given by the sum of a diffusion term and a sedimentation term.

In the measurement of optical absorbance (or transmission), the Lambert Beer law is used:

$$\log_{10}(I / I_0) = -\varepsilon c l \tag{9}$$

where I/I_0 is the intensity ratio, ε is the extinction coefficient, c is the concentration and l is the path length. The extinction coefficient depends on the molar mass concentration and the properties of the molecular species. Modern instrumentation allows simultaneous analysis of space and time extinction profiles (STEP spectra) as explained in the next section.

2. Techniques and Analyses

2.1 Experimental

For the purpose of explaining modern AC equipment and methods, measurement of STEP spectra will be shown taken from a LumiSizer 651 instrument (LUM GmbH, Berlin). The LumiSizer has 2500 sensors that detect light at approximately 14 μm intervals along the length of polyacrylamide or polycarbonate cells and records profiles simultaneously at regular time intervals with a rotor radius of 0.13 m. Figure 1 shows an example of AC measurements for SiO_2 using SepView 6.

A traditional method to analyze data in Fig. 1a would be to take the midpoint of each profile and to plot it versus time to give an average sedimentation coefficient and an average concentration at the midpoint. With modern instrumentation, the histogram of extinction-weighted sedimentation velocity profiles based on no assumptions are given by Fig. 1b and direct use of eq. (5) gives the particle size distribution (Fig. 1c). Lerche [6] gives many examples of *in situ* sedimentation measurement and analysis with examples of monomodal monodisperse suspensions, tetramodal monodisperse suspensions, polydisperse suspensions, flocculated suspensions, emulsions, suspo-emulsion (flotation and sedimentation), latex, polystyrene, pectin gels, magnetite including techniques that use monodisperse tracers to probe the structure of gels or magnets to study the interactions in ferrofluids.

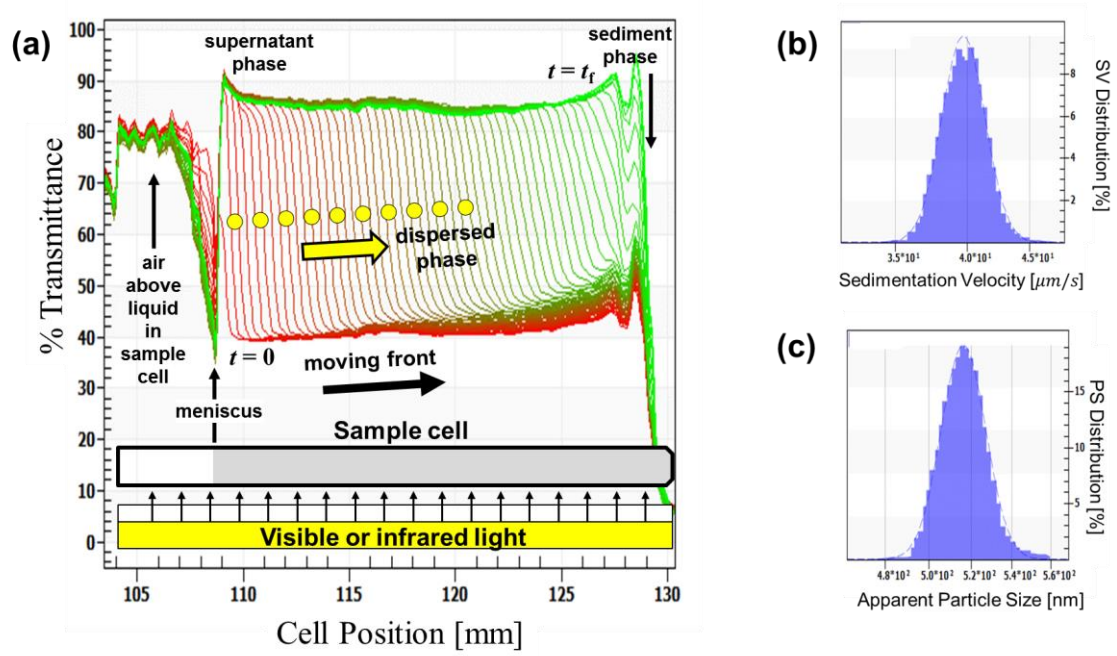

Figure 1. Space-time extinction profiles (STEP spectra) for SiO_2 nanoparticles (d = 500 nm, c = 0.11 wt%, λ = 870 nm, RCF = 327) in water at 25 °C obtained from an analytical centrifuge at 1500 rpm showing (a) STEP spectra showing approximate midpoint of some profiles of the moving front as yellow circles, (b) sedimentation velocity (SV) histogram and (c) apparent particle size (PS) distribution for ρ_P = 2000 kg/m^3. Color coding shows progression from red (t = 0) to green (t = t_f, final time) at approximate 10 s intervals.

The application of AC/AUC to nanoparticles is of interest for determining their physical properties. Carney et al. [3] determined nanoparticle size distribution with either density or molecular weight (M) by using 2D AUC and the following relationships that were obtained by re-expressing eq. (2) and by using the Stokes-Einstein relationship:

$$\rho_P = \rho_S + 18 \cdot \mu_S \cdot s \cdot \left(\frac{1}{D} \cdot \frac{k_B T}{3\pi\mu_S} \right)^{-2} \tag{10}$$

$$M = \frac{sRT}{D} \left(1 - \frac{\rho_S}{\rho_P} \right)^{-1} \tag{11}$$

$$d_h = d_P = \sqrt{\frac{18\mu_S s}{(\rho_P - \rho_S)}} \tag{12}$$

and assuming that $d_h = d_P$ and using two of the three variables (M, d_P, ρ_P) as fitting parameters. In their procedure, they solved the Lamm equation (eq. (8)) using SEDFIT software [7] to obtain families of curves of sedimentation coefficients and diffusion coefficients, that is, in two

dimensions, *s* and *D*. They examined several types of nanoparticle systems: (i) single monodisperse standard nanoclusters of magic-sized gold thiolates, $Au_{144}(SCH_2CH_2C_6H_6)_{60}$, (ii) mixtures of three nanocluster standards, $Au_{25}(SCH_2CH_2C_6H_6)_{18}$TOA, $Au_{38}(SCH_2CH_2C_6H_6)_{24}$, and $Au_{144}(SCH_2CH_2C_6H_6)_{60}$, where TOA refers to tetraoctylammonium ion, (iii) pentadecanethiol (PDT) coated gold NPs (ρ_{Au} = 19320 kg/m^3; ρ_{PDT} = 850 kg/m^3) and (iv) polydisperse gold nanoparticles, sodium 11-mercaptoundecanesulfonate-capped AuNPs (MUS-NPs), with core diameters (4 to 9) nm. For the case of (i) magic-sized gold clusters, ρ_P was determined from weight-averaged diffusion and sedimentation coefficients using eq. (10) and then eq. (11) allowed calculation of molecular weight and finally eq. (12) was used to calculate d_P. Results agreed well with ESI-MS methods to within a few percent and the authors were able to resolve the mixture of nanocluster standards, case (ii) as well. For the PDT-coated gold NPs, case (iii), the authors were able to resolve the shell thickness and show that AUC could distinguish between a unimodal and a bimodel distribution, which was difficult to estimate with scanning electron microscopy. For polydisperse gold samples, however, there were some limitations brought out by variation of shape, for example particles with rods of different shapes. Nevertheless, the method shows the determination of size, density and molecular weight of NPs without the use of standards or auxiliary measurements.

3. Application to Phase Equilibria

AC/AUC have many potential applications in estimating the thermodynamic parameters of complicated molecular species and in the determination of phase equilibria or elucidation of molecular interactions. This section describes some of the areas where centrifugation has been used as an analytical tool as part of the experimental method or a process unit operation. For example, process intensification with centrifugal contactors that is highlighted at the end of this section, is making it possible to achieve high reaction or separation efficiencies in compact devices and they have been evaluated favorably economically for large-scale applications (e.g. see ore processing).

3.1 Osmotic pressure equation of state

The osmotic pressure equation of state (EoS) is key to being able to describe the phase behavior of many different types of colloidal systems, since the osmotic pressure represents the chemical potential and must be equal between biphasic regions that contains a nanoparticle or colloidal system. The osmotic pressure EoS can be determined by measuring the sedimentation equilibrium with AC.

3.1.1 Ferrofluids

Luigjes et al. [8] determined the osmotic pressure equation of state of ferrofluids by

measuring their sedimentation equilibrium with AC. Monodisperse colloidal magnetic Fe_3O_4 (magnetite) nanoparticles were denoted as S-particles (11 nm, oleic acid coating) and L-particles (13.4 nm, oleic acid coating) that were dispersed in 15.6 mM oleic acid in decalin solutions. Data reduction used the following relationship to obtain the osmotic pressure, Π:

$$\Pi(r') = \omega^2 \Delta m \int_{r,\,\rho\to 0}^{r'} \rho(r) \cdot r dr \tag{13}$$

where Δm is the colloidal particle buoyant mass, ρ is the particle number concentration and ω is the angular velocity. Those authors compared results to the well-known van't Hoff relation ($\Pi = \rho RT$) and to one based on hard sphere repulsion described by the Carnahan-Starling equation of state:

$$\Pi = \rho RT \left(\frac{1 + \phi + \phi^2 - \phi^3}{(1-\phi)^3} \right) \tag{14}$$

where ϕ is the colloidal volume fraction. There were several important findings [8, 9]:

1. The AC technique allowed reliable measurement of extremely low osmotic pressures (ca. 3 Pa) and determination of osmotic second virial coefficients.
2. The S-particles exhibited osmotic pressure behavior close to the van't Hoff relation while the L-particles exhibited significant deviations from the van't Hoff relation. The osmotic pressures of both types of particles were much lower than the hard-sphere values, eq. (14). The L-particles had significantly negative second virial coefficients indicating strong nonidealities.
3. Even though there is only a small difference in the diameters between the S-particles and L-particles (e.g. 2.4 nm), there was a large difference in their coupling constants (λ=2.0-2.4 for L-particles versus λ =1.1-1.3 for S-particles) indicating strong size dependence of the dipolar coupling constant.

The method developed by Luigjes et al. [8, 9] shows that AC can be used to assess dipolar attractions in ferrofluids and that AC analyses have wide application to both magnetic and semiconductor nanoparticles.

3.1.2 Synthetic clay

AC/AUC can be used to measure sedimentation equilibrium, which allows determination of the osmotic pressure EoS via eq. (13). Page et al. [10] used AUC and determined the EoS for a synthetic clay laponite ($Si_8Mg_{5.45}Li_{0.4}H_4O_{24}Na_{0.7}$) in the cetyltrimethylammonium–myristate–water system for which the phase behavior is well-known. A chief advantage of AUC over other techniques for measuring the phase behavior of colloidal systems is that a large concentration range can be measured in a single sedimentation equilibrium experiment. Furthermore, AUC allows access to regions of small pressure

differences by changing AUC parameters (e.g. rpm) and access to several phases or phase boundaries in a single measurement.

3.2 Asphaltene nanoaggregates

Asphaltenes exhibit nanoaggregation which does not occur for crude oil resins [11] and moreover, the nanoaggregates greatly affect physical properties such that a critical nanoaggregate concentration (CNAC) can be defined. Mostowfi et al. [11] used AUC to both verify the existence of nanoaggregates and to determine changes in the asphaltene aggregation profiles at concentrations above and below the CNAC. Those authors found that aggregation profiles were consistent with a CNAC of 50 mg/L in toluene and that the nanoaggregate size was 2.5 nm with monomer sizes being less than 1.5 nm in agreement with diffusion measurements. Moreover, Mostowfi et al. [11] developed a phase equilibrium model for the deposit of asphaltenes from solution thus linking the AUC results with the solid-liquid phase equilibria of the system.

3.3 Deep Eutectic Solvent Phase Diagrams

Deep eutectic solvents (DES) are ionic solvent systems that form when Lewis or Brønsted acids are combined with bases to give a lower melting point compound than that of the pure components. DES are readily made from renewable compounds, are inexpensive and have been proposed for a wide range of applications [12-14]. However, since DES are not molecular solvents, their solid-liquid equilibria (SLE) are needed for application. Although solid-liquid equilibria of DES can be measured with synthetic or dynamic techniques, they do not readily crystallize and they may supercool to a metastable liquid phase [15] making determination of their SLE time-consuming and unreliable. To avoid the crystallization step and to improve both data reliability and measurement efficiency, van den Bruinhorst et al. [15] proposed a method to measure SLE of DES that used centrifugation. In that method, mixtures were only partially liquefied and kept at constant temperature and then centrifuged before being sampled. Although the researchers did not use AC for the measurements, they were able to verify that their centrifugation method gave reliable data for a binary eutectic system (bibenzyl-biphenyl) and for DES (urea-choline chloride). In the procedure, it is likely that AC can be used to confirm sedimentation times required for measuring equilibria and for rapid analysis of compositions subject to their optical properties.

3.4 Nanoparticle - Surfactant Interactions

Esmaeilzadeh et al. [16] studied the effect of ZnO_2 nanoparticles on the interfacial behavior of surfactant solutions of air-water and n-heptane-water systems. Anionic surfactant (sodium dodecyl sulfate, SDS), cationic surfactant (dodecyl trimethyl ammonium bromide,

C_{12}TAB) and nonionic surfactant (lauryl alcohol 7 mole ethoxylate, LA7) were used. Although the researchers used centrifugation of solutions above and below the critical micelle concentration (CMC), the procedures were tedious to determine the adsorbed surfactant on the nanoparticles, which could be most likely inferred from AC measurements and the estimation of the hydrodynamic diameters of the NPs in solution with and without surfactants.

3.5 Colloidal crystallization

Opal is a colloidal crystal that has photonic properties and forms from the close packing of amorphous SiO_2 after years of sedimentation and compression in the earth. Synthetic opal and inverse opal structures have many potential applications in photonics for developing all-optical integrated circuits and energy storage devices [17].

Centrifugation is one method that has been proposed to speed up the natural process of colloidal crystallization [18]. Suzuki et al. [18] used a dispersion of polystyrene particles in KCl with centrifugation of 82 G, 185 G and 329 G. As a result, they found that they could increase the grain size to 0.3 mm in width and 8 mm in length with the largest growth rate being for the highest applied centrifugal force [18]. Although the authors used an optical cell in the measurements, self-assembly of the polystyrene particles was not followed *in situ*, whereas with use of AC, it would be possible to estimate critical concentrations for crystallization and other aspects of the mechanism.

3.6 Centrifugal contactor separators (CCSs)

Centrifugal contactors mix, contact and separate two immiscible phases of different densities via a rotational force on a mass ($F=m\omega^2 r$). One of the first works that proposed centrifugal contactors as reactors was proposed by Kraai et al. [19], who studied the production of biodiesel from sunflower oil, methanol and sodium methoxide ($NaOCH_3$). In the centrifugal contactor reactor, the key parameters were the rotational force, F, and the residence time in *g*-seconds, which is the period that the reacting phases maintain contact in the centrifugal field.

Table 1 shows selected applications that have proposed CCSs in the areas of energy (Entry 1), environment (Entries 2-5), nanotechnology (Entry 6) and pharmaceuticals (Entries 7-9). Ilmi et al. [20] used immobilized enzymes in CCSs to produce FAMEs from sunflower oil and methanol. Under batch conditions, 95% yields of FAMEs could be obtained, but this dropped to 85% under continuous mode (Table 1), but nevertheless, it showed the potential of using an immobilized enzyme with the CCS device.

Modak et al. [21] studied the removal of methyl red from an aqueous stream with xylene solvent in CCSs (Table 1, Entry 2). According to the results, high efficiency could be obtained, but at a solvent/feed ratio of 10. Still, one of the interesting findings was that the CCS allowed

reactor volume to be reduced by an order of magnitude due to the efficiency of the CCS device.

Usually CCSs are applied to two immiscible liquid phases. However, MacInnes et al. [22] studied the application of CCS to a gas-liquid stream for CO_2 gas capture (Table 1, Entry 3). Although the researchers used a model gas stream that was rich in CO_2, they could remove 90% of the CO_2 with a moderate RCF value.

As another example of CCS being applied to a non-liquid-liquid system (Table 1, Entry 4), Jang et al. [23] studied the recovery of rare earth elements (REE) from phosphoric acid sludge. Here, the waste stream contained 54% P_2O_5 as a highly viscous liquid with a large (*ca.* 40%) solid content. A CCS system was designed and it was found that up to 94% of the solids could be recovered at RCF values of 2235 with the solids containing from (1500 to 2895) ppm REE. Scale-up of the design to 50,000 tons/a at a site in Florida (U.S.A.) showed favorable economics for processing of the ore.

In an environmental study (Table 1, Entry 5), Jing et al. [24] used CCS for leaching of vanadium (V) from vanadium (V) - chromium (VI) solutions. By using a leaching solution that contained N1923 (C_{19}-C_{23} secondary alkyl primary amines), V(V) could be obtained in high recovery and 100% selectivity with either three or four stages of the CCS devices. The ideal contact time in the CCS was determined to be 3.6 min.

The classification of silica nanoparticles is important for nanotechnology development. Konrath et al. [25] studied the classification of fumed silica nanoparticles (d=75 nm) with a disk type AUC (Table 1, Entry 6). In that research, they also employed an AC device to study particle interactions. According to their results, roughly 74% of the particles at 50 nm could be classified at RCF values of 9600 or 38500.

Pharmaceutical industries have much to gain by using CCSs for processing pharmaceuticals (Table 1, Entries 7-9) to obtain high enantiomeric efficiencies (ee). Schuur et al. [26] and Xu et al. [27] show fair results for chiral separations (Entries 7-8). From the one-stage results of Xu et al. [27], 60 stages would be needed for 97% ee and 82 stages would be needed for 99% ee, thus the choice of the host makes a large difference in the ee obtained.

Zhang et al. [28] studied the separation of (S)-propranolol from (R)-propranolol by fractional extraction with CCSs (Table 1, Entry 9). Propranolol is a pharmaceutical used for treatment of arrhythmias (heart flutter) and the (S) form is 100 times as potent as the (R) form. A model was developed and used for the actual 10 CCSs based on achieving equilibrium and it was found that 98% ee could be obtained for (S)-propranolol, whereas 25 CCSs could achieve 98% ee and 99% yields.

In consider the above applications, if AC is used, both F and g-seconds of a small (cuvette) system can be determined based on the rate of turbidity changes of the two phases and the time required for phases to separate under a given RCF value. Thus initial conditions for centrifugal contactor devices can most likely be reliably estimated with AC measurements.

Table 1. Selected research studies that have proposed centrifugal contactor separators (CCSs) for applications in energy, environment, nanotechnology and pharmaceutical areas. Relative centrifugal force (RCF) given by eq. (1).

Entry	Application	Target	Result	Rotating Geometry	Max RCF	Ref.
1	Biodiesel production from sunflower oil and methanol with immobilized enzyme	fatty-acid methyl esters (FAMEs)	85% yield (continuous)	cylinder	180	[20]
2	Removal of methyl red from water with xylene solvent	methyl red	98% recovery at S/F=10	cylinder	180	[21]
3	CO_2 capture from 90 mol CO_2:10 mol N_2 gas stream with diethanolamine-water	CO_2/low solvent use	90% CO_2 recovery	spiral	306	[22]
4	Phosphoric acid sludge from ore processing, 54% P_2O_5, 30-40% solids	Rare earth element (REE) recovery	94% solids recov. ~2800 ppm REE	cylinder	2235	[23]
5	Vanadium (V) and chromium (VI) separation with primary amine N1923	Vanadium(V)	95.1% V 100% selectivity	cylinder	306	[24]
6	Silica nanoparticle (NP) classification (Aerosil 200 fumed silica), d=75 nm feed	d=50 nm NP fraction	74% yield	disk	38500	[25]
7	Amino acid derivatives enantioseparation using host cinchona alkaloid	3,5-dinitrobenzoyl-leucine	55% yield 98% ee	cylinder	580	[26]
8	Chiral separation by host hydroxyethyl-β-cyclodextrin	2-phenylbutyric acid	42% ee, 1-stage 99% ee, 82-stages	cylinder	513	[27]
9	Separation of propranolol by fractional extraction and host dicyclohexyl D-tartrate	propranolol enantiomers	98% yield 98% ee	cylinder	513	[28]

4. Conclusions

Analytical centrifugation (AC) and analytical ultracentrifugation (AUC) are now standard techniques for studying proteins, biological molecules and polymers and are beginning to be applied to nanotechnology, materials and chemical sciences. AC and AUC techniques allow the rapid determination of the properties of molecular species in their native solutions and provide insight into the molecular interactions of colloidal systems. AC and AUC techniques have application in fluid phase equilibria through the determination of osmotic pressure equations of state, adsorption equilibria, surfactant-containing systems, solid-liquid equilibria of viscous systems and design of centrifugal reactors and separators. The use of AC/AUC will broaden the scope of chemical systems that can be studied and will stimulate research in fluid phase equilibria.

Acknowledgments

The authors would like to acknowledge financial support for this research from the Materials Processing Science project ("Materealize") of the Ministry of Education, Culture, Sports, Science and Technology (MEXT), Grant Number JPMXP0219192801.

References

[1] T. Svedberg, H. Rinde, J. Am. Chem. Soc., 46 (1924) 2677-2693.
[2] D.J. Winzor, V. Dinu, D.J. Scott, S.E. Harding, Biophysical Reviews, 13 (2021) 273-288.
[3] R.P. Carney, J.Y. Kim, H. Qian, R. Jin, H. Mehenni, F. Stellacci, O.M. Bakr, Nat Commun, 2 (2011) 335.
[4] M.J. Uttinger, D. Jung, N. Dao, H. Canziani, C. Lübbert, N. Vogel, W. Peukert, J. Harting, J. Walter, Soft Matter, 17 (2021) 2803-2814.
[5] J. Walter, T. Thajudeen, S. Süβ, D. Segets, W. Peukert, Nanoscale, 7 (2015) 6574-6587.
[6] D. Lerche, KONA Powder and Particle Journal, 36 (2019) 156-186.
[7] P. Schuck, R.B. Gillis, T.M.D. Besong, F. Almutairi, G.G. Adams, A.J. Rowe, S.E. Harding, Analyst, 139 (2014) 79-92.
[8] B. Luigjes, D.M.E. Thies-Weesie, A.P. Philipse, B.H. Erné, Journal of Physics Condensed Matter, 24 (2012).
[9] B. Luigjes, D.M.E. Thies-Weesie, B.H. Erné, A.P. Philipse, Journal of Physics Condensed Matter, 24 (2012).
[10] M.G. Page, T. Zemb, M. Dubois, H. Colfen, Chemphyschem, 9 (2008) 882-890.
[11] F. Mostowfi, K. Indo, O.C. Mullins, R. McFarlane, Energy & Fuels, 23 (2009) 1194-1200.
[12] O.A.O. Alshammari, G.A.A. Almulgabsagher, K.S. Ryder, A.P. Abbott, Green Chemistry,

23 (2021) 5097-5105.
[13] G. Di Carmine, A.P. Abbott, C. D'Agostino, Reaction Chemistry and Engineering, 6 (2021) 582-598.
[14] I.M. Pateli, A.P. Abbott, G.R.T. Jenkin, J.M. Hartley, Green Chemistry, 22 (2020) 8360-8368.
[15] A. van den Bruinhorst, L. Kollau, M.C. Kroon, J. Meuldijk, R. Tuinier, A.C.C. Esteves, J Chem Phys, 149 (2018) 224505.
[16] P. Esmaeilzadeh, N. Hosseinpour, A. Bahramian, Z. Fakhroueian, S. Arya, Fluid Phase Equilibria, 361 (2014) 289-295.
[17] E. Armstrong, C. O'Dwyer, Journal of Materials Chemistry C, 3 (2015) 6109-6143.
[18] Y. Suzuki, T. Sawada, K. Tamura, Journal of Crystal Growth, 318 (2011) 780-783.
[19] G.N. Kraai, F. van Zwol, B. Schuur, H.J. Heeres, J.G. de Vries, Angewandte Chemie International Edition, 47 (2008) 3905-3908.
[20] M. Ilmi, A. Kloekhorst, J.G.M. Winkelman, G.J.W. Euverink, C. Hidayat, H.J. Heeres, Chemical Engineering Journal, 321 (2017) 76-85.
[21] J.B. Modak, A. Bhowal, S. Datta, Journal of Hazardous Materials, 304 (2016) 337-342.
[22] J.M. MacInnes, A.A. Ayash, G.R.M. Dowson, Chemical Engineering Journal, 307 (2017) 1084-1091.
[23] G.G. Jang, A. Ladshaw, J.K. Keum, P. Zhang, C. Tsouris, Industrial and Engineering Chemistry Research, 59 (2020) 21901-21913.
[24] X. Jing, P. Ning, H. Cao, Z. Sun, J. Wang, Chemical Engineering Journal, 315 (2017) 373-381.
[25] M. Konrath, A.-K. Brenner, E. Dillner, H. Nirschl, Separation and Purification Technology, 156 (2015) 61-70.
[26] B. Schuur, A.J. Hallett, J.G.M. Winkelman, J.G. De Vries, H.J. Heeres, Organic Process Research and Development, 13 (2009) 911-914.
[27] W. Xu, G. Dai, K. Tang, P. Zhang, B. Xiong, Y. Liu, Separation and Purification Technology, 179 (2017) 53-60.
[28] P. Zhang, W. Xu, K. Tang, Organic Process Research and Development, 22 (2018) 1782-1792.